Kinetics and Thermodynamics of Small Molecule Binding to Pincer-PCP Rhodium(I) Complexes

Mark D. Doherty,[†,§] David C. Grills,*[,†] Kuo-Wei Huang,[†,∥] James T. Muckerman,[†] Dmitry E. Polyansky,*[,†] Rudi van Eldik,[‡] and Etsuko Fujita*[,†]

[†]Chemistry Department, Brookhaven National Laboratory, P.O. Box 5000, Upton, New York 11973-5000, United States
[‡]Department of Chemistry and Pharmacy, University of Erlangen-Nürnberg, Egerlandstrasse 1, 91058 Erlangen, Germany

Ⓢ Supporting Information

ABSTRACT: The kinetics and thermodynamics of the binding of several small molecules, L (L = N_2, H_2, D_2, and C_2H_4), to the coordinatively unsaturated pincer-PCP rhodium(I) complexes $Rh[^tBu_2PCH_2(C_6H_3)CH_2P^tBu_2]$ (**1**) and $Rh[^tBu_2P(CH_2)_2(CH)(CH_2)_2P^tBu_2]$ (**2**) in organic solvents (n-heptane, toluene, THF, and cyclohexane-d_{12}) have been investigated by a combination of kinetic flash photolysis methods, NMR equilibrium studies, and density functional theory (DFT) calculations. Using various gas mixtures and monitoring by NMR until equilibrium was established, the relative free energies of binding of N_2, H_2, and C_2H_4 in cyclohexane-d_{12} were found to increase in the order $C_2H_4 < N_2 < H_2$. Time-resolved infrared (TRIR) and UV−vis transient absorption spectroscopy revealed that 355 nm excitation of **1−L** and **2−L** results in the photoejection of ligand L. The subsequent mechanism of binding of L to **1** and **2** to regenerate **1−L** and **2−L** is determined by the structure of the PCP ligand framework and the nature of the solvent. In both cases, the primary transient is a long-lived, unsolvated species ($\tau = 50 - 800$ ns, depending on L and

its concentration in solution). For **2**, this so-called less-reactive form (LRF) is in equilibrium with a more-reactive form (MRF), which reacts with L at diffusion-controlled rates to regenerate **2−L**. These two intermediates are proposed to be different conformers of the three-coordinate (PCP)Rh fragment. For **1**, a similar mechanism is proposed to occur, but the LRF to MRF step is irreversible. In addition, a parallel reaction pathway was observed that involves the direct reaction of the LRF of **1** with L, with second-order rate constants that vary by almost 3 orders of magnitude, depending on the nature of L (in n-heptane, $k = 6.7 \times 10^5$ M^{-1} s^{-1} for L = C_2H_4; 4.0×10^6 M^{-1} s^{-1} for L = N_2; 5.5×10^8 M^{-1} s^{-1} for L = H_2). Experiments in the more coordinating solvent, THF, revealed the binding of THF to **1** to generate **1−THF**, and its subsequent reaction with L, as a competing pathway.
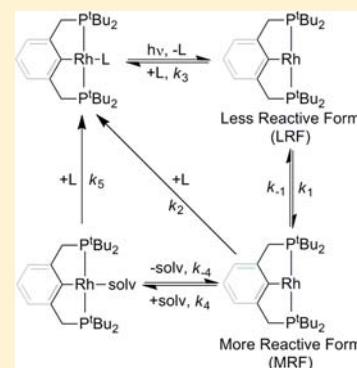
■ INTRODUCTION

The activation of small molecules (e.g., N_2, H_2, CO_2, etc.) by transition metal centers has attracted a considerable amount of attention since these types of reactions are often relevant to catalytic processes such as nitrogen fixation and CO_2 reduction. In many cases, an initial coordination of the small molecule to a coordinatively unsaturated metal complex occurs. Effective catalyst development therefore requires a thorough understanding of the kinetic and thermodynamic barriers associated with such substrate or ligand binding reactions.

UV−vis transient absorption and time-resolved infrared (TRIR) studies have shown that, in the gas phase, in the absence of an intramolecular agostic interaction, the vacant site of a coordinatively unsaturated transition metal complex **II** (formed by photoejection of a ligand from **I** in Scheme 1) remains unoccupied. The binding of small molecules to this vacant site is thus extremely fast, with bimolecular rate constants typically on the order of 10^{10} M^{-1} s^{-1} (k_1 in Scheme 1).[1−4] However, in solution these unsaturated complexes are often weakly coordinated via a σ-interaction from a solvent molecule[5−14] (**II** to **IIIa**, k_2 in Scheme 1), or stabilized through an internal agostic interaction[15,16] (**II** to **IIIb**, k_3 in Scheme 1)

Scheme 1. Some of the Possible Reaction Pathways for a Coordinatively Unsaturated Metal Complex (II) Generated by Photoejection of a Ligand L, Showing the Formation of Solvated (IIIa), Agostic (IIIb), and C−H Activated (IIIc) Intermediates, and Their Reactions with L To Regenerate the Original Complex
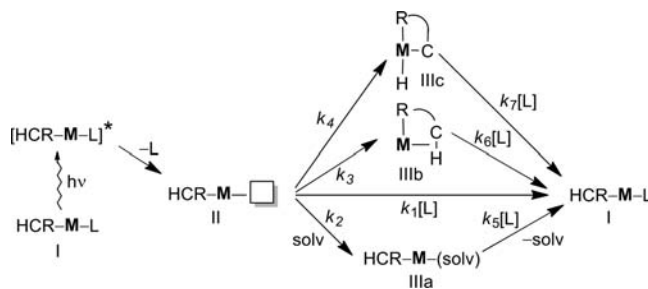
within picoseconds of their formation, either of which may or may not lead to a C−H activated product (e.g., **IIIc** in Scheme 1). Most solvents will bind to the vacant site of a metal center via these weak σ-interactions, even apparently inert solvents such as hydrocarbons.[6,8−10,17−21] Although weak when compared to a covalent bond, the interaction is real and measurable, with binding energies on the order of 5−15 kcal mol^{-1}.[1,3,4,8,15,22−24] The breaking of the M−solvent (or agostic) bond is thus an important factor, and the binding rates of small molecules in solution decrease by several orders of magnitude, with typical bimolecular rate constants in the 10^5−10^8 M^{-1} s^{-1} range (k_5, k_6, or k_7 in Scheme 1).[2,8,18−21]

There are, of course, exceptions to this generalized model of ligand binding to photogenerated coordinatively unsaturated metal complexes. For example, some species that are ground state triplets, such as Cp′Co(CO) (Cp′ = η^5-C$_5$H$_5$ or η^5-C$_5$(CH$_3$)$_5$),[22,25,26] and (PNP)Co (PNP = (^{t}Bu$_2$PCH$_2$SiMe$_2$)$_2$N),[27,28] show no evidence for solvent coordination and exhibit low rate constants for the binding of small molecules. Another photogenerated triplet fragment, ^{3}Fe(CO)$_4$, exhibits an unusually long lifetime in solution (τ = 12 ns) in its reaction with n-heptane to form ^{1}Fe(CO)$_4$(n-heptane).[29] There are also singlet species that show no evidence for solvent coordination, e.g., a family of square-planar MP$_4$ complexes (M = Ru or Os; P$_4$ = dmpe, depe, dfepe, dppe, or P(CH$_2$CH$_2$PPh$_2$)$_3$), generated upon photolysis of the dihydrides, MP$_4$H$_2$, which subsequently react directly with incoming ligands, such as CO, H$_2$, and C$_2$H$_4$ via second order kinetics.[30−35]

For some time we have been interested in the coordination and activation of CO$_2$, H$_2$, and other small molecules by late transition metal centers with respect to the development of effective pathways for their conversion into ultimately more desirable species such as liquid fuels and ammonia.[36−46] Late transition metal complexes bearing PCP-type pincer ligands have been employed in a variety of chemical transformations[47] including hydrogen transfer reactions,[48−56] C−X bond activation reactions,[57−60] and C−C coupling reactions[61−66] due to the ease with which the PCP ligand can be modified to control catalyst stability, reactivity, and selectivity.[51,52] In particular, the PCP-pincer rhodium dihydrogen complexes **1−H$_2$** and **2−H$_2$** (L = H$_2$ in Chart 1) have been reported to

Chart 1. PCP-Pincer Rhodium(I) Complexes
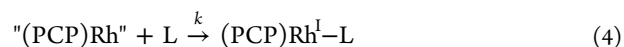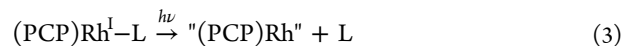

1−L   2−L
Kaska, 1988   Milstein, 1996
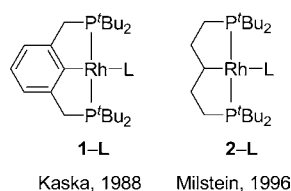
reduce CO$_2$ stoichiometrically at room temperature to generate a rhodium(III) hydrido formate complex, which in the case of **1−H$_2$** reacts further to produce CO and H$_2$O in a reverse water-gas shift type reaction.[45,67,68] While **1−H$_2$** and **2−H$_2$** can activate CO$_2$ via insertion of CO$_2$ into the Rh−H bond, only the formation of **2−CO$_2$** has been reported.[68] Such a difference in reactivity might be due to stronger σ-donor and/or π back-bonding interactions between Rh and C (phenyl) in **1−L**, which may weaken the Rh−CO$_2$ bond in **1−CO$_2$**.

$$(PCP)Rh^I-L + L' \overset{K_{ex}}{\rightleftharpoons} (PCP)Rh^I-L' + L \tag{1}$$

$$\Delta G^\circ_{rel.bind} = -RT \ln(K_{ex}) \tag{2}$$

The relative equilibrium binding strengths of various small molecule ligands, L/L′ (eqs 1 and 2) to complex **2** were determined by Milstein and co-workers using high-pressure NMR equilibrium methods to be in the order L = H$_2$ > N$_2$ > C$_2$H$_4$ > CO$_2$.[68]

$$(PCP)Rh^I-L \overset{h\nu}{\rightarrow} \text{"}(PCP)Rh\text{"} + L \tag{3}$$

$$\text{"}(PCP)Rh\text{"} + L \overset{k}{\rightarrow} (PCP)Rh^I-L \tag{4}$$

In an effort to further understand the differences between complexes **1** and **2** in terms of their reactivity with small molecules, and to gain mechanistic and kinetic insight into these ligand binding reactions, we have used a combination of high-pressure NMR equilibrium studies, time-resolved UV−vis and infrared spectroscopy (eqs 3 and 4), pressure-dependent kinetics, and DFT calculations to determine both the equilibrium and kinetic binding affinities of L = H$_2$, D$_2$, N$_2$, and C$_2$H$_4$ to the coordinatively unsaturated complexes **1** and **2**. This has resulted in the discovery of long-lived unsolvated forms of **1** and **2**, with lifetimes on the order of 50−800 ns, depending on the identity of L and its concentration in solution. Although the precise structure of these species remains unknown, it is proposed that they are stabilized by the adoption of a particular conformation of the three-coordinate (PCP)Rh fragment that exhibits diminished reactivity (or in the case of **2**, no reactivity) with L. Other factors such as agostic stabilization, blocking of the coordination site by solvent, and spin state changes, are also considered. A much more reactive form of **1** and **2** is generated from the initial long-lived form, and the mechanism of the subsequent reactivity with L and/or solvent molecules is dictated by the structure of the PCP ligand and the nature of the solvent.

■ EXPERIMENTAL SECTION

General. **1−N$_2$** and **2−N$_2$** were synthesized according to literature procedures.[68,69] All manipulations were carried out in a drybox under dinitrogen, and solid samples were transferred to a high vacuum line for solution preparations. Research grade N$_2$, H$_2$, D$_2$, and ethylene (from Praxair) were used without further purification. HPLC grade hexanes and THF were purified in the published manner[70] and stored under vacuum over NaK. HPLC grade toluene and n-heptane were distilled prior to use and stored under vacuum over NaK.

Heptane solutions for UV−vis transient absorption spectroscopy experiments were typically prepared at concentrations of ∼5−8 × 10^{-5} M by adding a small amount of solid **1−N$_2$** or **2−N$_2$** to a high-vacuum quartz UV−vis cuvette specially adapted with a side arm bulb and Swagelok valve (SS-4H). The solvent was then vacuum transferred into the side arm bulb under high-vacuum, the vapor pressure of the solvent recorded, and then a known pressure of gas L added to the solution to generate **1−L** or **2−L**. If L ≠ N$_2$, the solution was typically degassed again by freeze−pump−thaw degassing (to remove all traces of N$_2$) and then L added again to a known pressure. Concentrations of gases in solution were calculated from literature data[71−74] and the measured partial pressure of L added (taking into account the solvent's vapor pressure). Throughout this Article the concentrations of dissolved gases in solution are reported. These concentrations can be converted back to partial gas pressures according to the following data, which are the concentrations of dissolved gas at a partial pressure of 1 atm at 25 °C: N$_2$ in n-hexane (10.67 mM),[72] N$_2$ in n-heptane (9.20 mM),[72] N$_2$ in THF (6.43 mM),[73] N$_2$ in toluene (5.37 mM),[72]

H$_2$ in n-heptane (4.66 mM),[72] H$_2$ in THF (3.38 mM),[74] D$_2$ in n-heptane (4.76 mM),[72] C$_2$H$_4$ in n-heptane (137.0 mM).[71] Toluene and THF solutions were prepared by a direct Na/Hg reduction of the Rh^{III} complex **1−(H)(Cl)** in solution under high vacuum in specially prepared glassware, again at concentrations of ∼5−8 × 10^{-5} M. The Na/Hg amalgam was held in a separate compartment (isolated by a frit), and the sample was gradually reduced with UV−vis spectral monitoring. Once the reduction was complete, and after removal of the Na/Hg compartment by flame sealing, the appropriate **1−L** complex was prepared by addition of gas L to the solution at a known pressure. Since the reduction reaction generates NaCl as a side product, which is not soluble in toluene, the suspended NaCl in the toluene solutions was allowed to settle to the bottom of the vessel before transient spectroscopic measurements were conducted. It should be noted that solutions of **1−L** and **2−L** are extremely oxygen sensitive. If there is a small leak and the solutions are exposed to air, they immediately decompose to a pale green solution of the dioxygen complex, **1−O$_2$**, the UV−vis spectrum of which is reported elsewhere.[75] All solutions for transient spectroscopy were prepared with recrystallized samples and purified solvents, and no impurities could be detected by NMR, UV−vis, and/or IR spectroscopy.

NMR Equilibrium Binding Studies. Equilibrium measurements were performed in 5 mm or 10 mm high-pressure NMR tubes (Wilmad 522-PV-7 and 513−7PVH-7). In a typical experiment, a solution of **1−N$_2$** or **2−N$_2$** in cyclohexane-d_{12} (3.8 × 10^{-4} to 6.5 × 10^{-3} M) was introduced into the high-pressure NMR tubes and degassed under high vacuum (10^{-5} to 10^{-6} Torr). Gas mixtures of various ratios (N$_2$:H$_2$ = 0.17, 0.55, 0.97, 1.74, 3.20; N$_2$:C$_2$H$_4$ = 1.06, 2.19) were prepared using a high pressure steel manifold at a total pressure of 5 atm and introduced into the degassed high pressure NMR tubes (the total pressure decrease was taken into consideration). The ratio of [Rh]−N$_2$ to [Rh]−H$_2$ or [Rh]−C$_2$H$_4$ complexes was monitored using ^{1}H NMR at 25 °C (for [Rh] = **1**, monitoring Ar−CH$_2$−P virtual triplet resonance at ∼3.2 ppm) or ^{31}P{^{1}H} NMR at 25 °C (for [Rh] = **2**, monitoring the ^{31}P doublet resonance), and equilibrium conditions were usually achieved within 1−2 h.

Transient Spectroscopy. Complete details of the instrumentation and techniques used for nanosecond time-resolved infrared (TRIR) spectroscopy, nanosecond (ns) and femtosecond (fs) UV−vis transient absorption spectroscopy, and transient absorption spectroscopy under high pressure are provided in the Supporting Information.

Computational Details. DFT calculations on **1**, **2**, and **1−L** were performed using the Gaussian 03 program (Revision E.01).[76] Geometry optimizations were performed using the default convergence criteria without any constraints. The B3LYP functional was used together with the LANL2DZ ECP basis set[77−79] for the Rh and P atoms and the all-electron D95 V basis set[80] for all other atoms in TD-DFT calculations and "preliminary" DFT geometry optimizations. Additional calculations to investigate possible agostic bonding were carried out at the B3LYP and MP2 levels of theory using the MWB28 ECP basis[81,82] for Rh and the 6-31G(d,p) basis[83,84] for all other elements. In order to obtain the final energies and geometries, further DFT calculations were carried out using the B3LYP/LANL2TZ(f) basis[77,85,86] for the Rh atom and the 6-311G(d) basis[87,88] for all other atoms. Frequency calculations were employed to characterize the stationary points as minima or transition state structures, to determine zero-point energies (ZPEs), and for free-energy calculations.

■ RESULTS

UV−Vis Spectroscopy. Dissolution of **1−N$_2$** or **2−N$_2$** in N$_2$-saturated n-hexane, n-heptane, toluene, or THF results in pale yellow solutions that exhibit similar UV−vis spectra. Since the N$_2$ ligand in **1−N$_2$** or **2−N$_2$** is easily displaced, the other **1−L** or **2−L** complexes under study (L = H$_2$, D$_2$, and C$_2$H$_4$) are readily generated by the addition of an appropriate pressure of gas L to a freeze−pump−thaw degassed solution of **1−N$_2$** or **2−N$_2$**, and subsequently repeating this procedure to obtain the other complexes. Figure 1 shows the UV−vis absorption
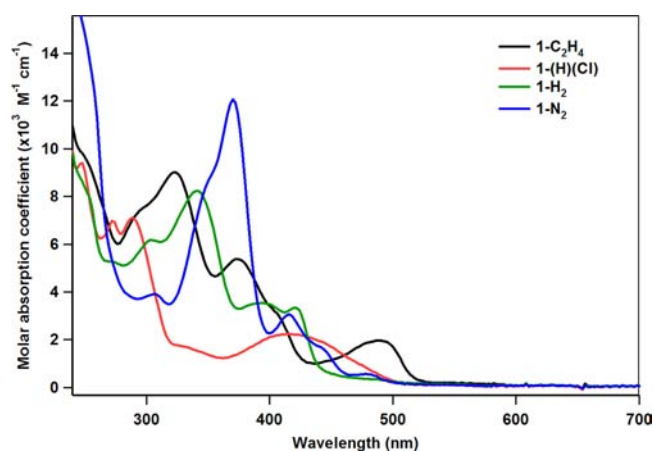

Figure 1. UV−vis absorption spectra of **1−L** complexes in n-hexane, obtained by Na/Hg reduction of **1−(H)(Cl)**, followed by addition of gas L. Each complex was prepared sequentially by freeze−pump−thaw degassing the solution followed by addition of a different gas L. Spectra in n-heptane, toluene, and THF are very similar. The spectrum of **1−(H)(Cl)** is also shown for comparison.

spectra of a series of **1−L** complexes (L = H$_2$, N$_2$, C$_2$H$_4$) and the spectra of **2−L** can be found in the SI (Figure S1). Each of these complexes exhibits a unique and characteristic UV−vis spectrum, apart from **1−D$_2$** (not shown), whose spectrum is identical to that of **1−H$_2$**. In contrast to other transition metal complexes containing small molecules as ligands, e.g., *mer,trans*-W(CO)$_3$(PCy$_3$)$_2$L (Cy = cyclohexyl),[15] the ligand L in **1−L** solutions cannot be removed by repeated freeze−pump−thaw degassing cycles, despite the fact that it can easily be exchanged by the addition of a different gas L. Band maxima and molar absorption coefficients for the complexes under study are presented in Table 1.

Table 1. Band Maxima (nm) and Molar Absorption Coefficients, ε (in parentheses, M^{-1} cm^{-1}) for 1−L in n-Hexane, and Band Maxima for 2−L Complexes in n-Heptane

complex	maxima (ε),[a] nm (M^{-1} cm^{-1})
1−(H)(Cl)	248 (6630), 272 (5060), 288 (5210), 422 (1680)
1−N$_2$	370 (12 100), 416 (3060), 444sh (1600), 478 (560)
2−N$_2$	334, 408, 422
1−H$_2$	304 (6180), 340 (8240), 394 (3550), 420 (33 400)
2−H$_2$	320, 400
1−C$_2$H$_4$	322 (9020), 374 (5380), 488 (1960)
2−C$_2$H$_4$	292, 350, 462
1−THF[b]	330, 386, 486

[a]ε's for **1−L** (L = N$_2$, H$_2$, and C$_2$H$_4$) were determined by assuming 100% conversion of **1−(H)(Cl)**. [b]In THF.

The UV−vis absorption spectrum of the Rh^I species generated after Na/Hg reduction of the Rh^{III} complex **1−(H)(Cl)** in freeze−pump−thaw degassed THF is assigned to the THF complex, **1−THF** (Figure S2). This is because the Rh^I species formed after two-electron reduction of **1−(H)(Cl)** will be very unstable, and is unlikely to exist as a three-coordinate species in the presence of a coordinating solvent. The reactive nature of this Rh^I species was confirmed by similar experiments in n-heptane. While the spectrum is very sensitive to the presence of a small amount of H$_2$ formed by the Na/Hg reduction, upon addition of N$_2$ to any of the n-heptane solutions after Na/Hg reduction, **1−N$_2$** was always formed

quantitatively. To further explore the nature of the Rh^I species in THF under these conditions, the Na/Hg reduction was repeated in THF-d_8 in a custom-built apparatus that allows NMR spectra of the solution to be recorded after the reduction reaction (see SI for details). ^1H NMR spectra taken between room temperature and −90 °C were consistent with a C_2 symmetric (PCP)Rh complex and showed no Rh−H peaks out to δ = −50 ppm. $^{31}P\{^1H\}$ NMR spectra taken over the same temperature range revealed a $^{103}Rh-^{31}P$ coupling constant ranging from 151 to 158 Hz, consistent with a rhodium(I) species.[89] Although ^{13}C NMR showed no strong evidence for a bound THF molecule, this is to be expected for a weakly bound solvent complex in which the solvent ligand is likely to be rapidly exchanging with other solvent molecules. A comparison with the NMR spectra of the separately prepared **1−N₂**, **1−H₂**, **1−O₂**, **1−CO**, and **1−CH₃CN** complexes (see SI) confirmed that no such species were formed in the Na/Hg reduction reaction in THF-d_8.

NMR Equilibrium Studies. In order to measure the relative binding free energies of ligands L to **1** (eqs 1 and 2), and also to compare with the relative binding free energies of L to the analogous complex **2**, reported by Milstein,[68] we performed a series of NMR equilibrium studies in cyclohexane-d_{12} (eq 5).

$$\text{(5)}$$
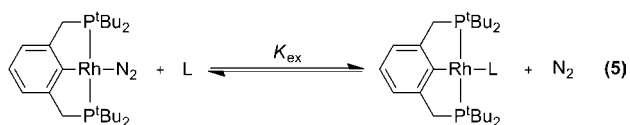
After pressurizing a degassed solution of **1−N₂** with various mixtures of N₂/H₂ or N₂/C₂H₄ at a total pressure of 5 atm, and monitoring the approach to equilibrium by NMR (see Experimental Section), the equilibrium constant, K_{ex}, for eq 5 was calculated from eq 6. This allowed the free energy change of the reaction to be calculated, which is equivalent to the difference in the free energies of binding of the incoming ligand L and the N₂ ligand to **1** (eq 2). The results are summarized in Table 2.

$$K_{ex} = \frac{[Rh-L][N_2]}{[Rh-N_2][L]} \qquad (6)$$

Table 2. Equilibrium Parameters Determined by NMR Spectroscopy in Cyclohexane-d_{12} at 25 °C for Equation 5

PCP complex	incoming ligand, L	K_{ex} (298 K)	ΔG°_{298}, kcal mol⁻¹
1−N₂	H₂	3.33 (±0.18)	−0.71 (±0.03)
1−N₂	C₂H₄	0.16 (±0.01)	+1.08 (±0.01)
2−N₂[a]	H₂	8.08 (±0.48)[a]	−1.24 (±0.04)[a]
2−N₂[a]	C₂H₄	0.07 (±0.001)[a]	+1.57 (±0.01)[a]

[a]These data were reported by Milstein and co-workers.[68]

Our experimental method was first validated by repeating Milstein's reaction of **2−N₂** with H₂ under H₂/N₂. The ΔG°_{298} we obtained for that reaction (−1.12 (±0.06) kcal mol⁻¹) was almost identical to that obtained by Milstein (−1.24 (±0.04) kcal mol⁻¹).[68] For complexes **1−L**, the trend in stability is the same as that previously observed for complexes **2−L**. Thus, formation of the **1−H₂** complex is slightly more favorable (−0.71 kcal mol⁻¹) than formation of the **1−N₂** complex, whereas C₂H₄ binding is less favorable than N₂ binding (+1.08 kcal mol⁻¹). However, the magnitudes of ΔG°_{298} for the

reactions involving **1** are smaller than for the corresponding reactions with **2**.

Ligand Dissociation from the Photoexcited States of 1−L and 2−L. Ligand dissociation from the photoexcited states of **1−L** and **2−L** was studied by time-resolved IR and UV−vis spectroscopies. Of all the complexes under study, only **1−N₂** and **2−N₂** were appropriate for investigation by TRIR spectroscopy, due to the strong ν_{NN} stretching band of the end-on bound N₂ ligand (2134 and 2118 cm⁻¹, respectively, in alkane solvent). The only transient feature observed after 355 nm laser flash photolysis of **1−N₂** in n-hexane in the presence of 21 mM N₂ was an instantaneous bleach of the ν_{NN} band at 2134 cm⁻¹, indicative of Rh−N₂ bond cleavage (Figure S3). The bleach band recovered completely with single exponential kinetics as the photoproduct reacted with N₂, with an observed rate constant (k_{obs}) of 1.3×10^6 s⁻¹. Very similar results were obtained for **2−N₂**, which exhibits a ν_{NN} band at 2118 cm⁻¹ in n-heptane, with the observed rate constant of recovery of **2−N₂** being 1.8×10^7 s⁻¹. The TRIR experiments thus confirmed that photoexcitation of a solution of **1−N₂** or **2−N₂** results in the photoejection of N₂, which then rebinds to **1** or **2** under pseudo-first-order conditions of excess N₂ to reform **1−N₂** or **2−N₂**. While no transient intermediates were identified from TRIR experiments, most likely due to their lack of IR activity, short-lived transient species were identified by laser flash photolysis using UV−vis detection.

Upon 355 nm laser flash photolysis of **1−N₂** or **2−N₂** in n-heptane in the presence of N₂, the transient absorption (TA) spectra shown in Figure 2 were recorded. An instantaneous formation of a strong transient absorption band in the visible
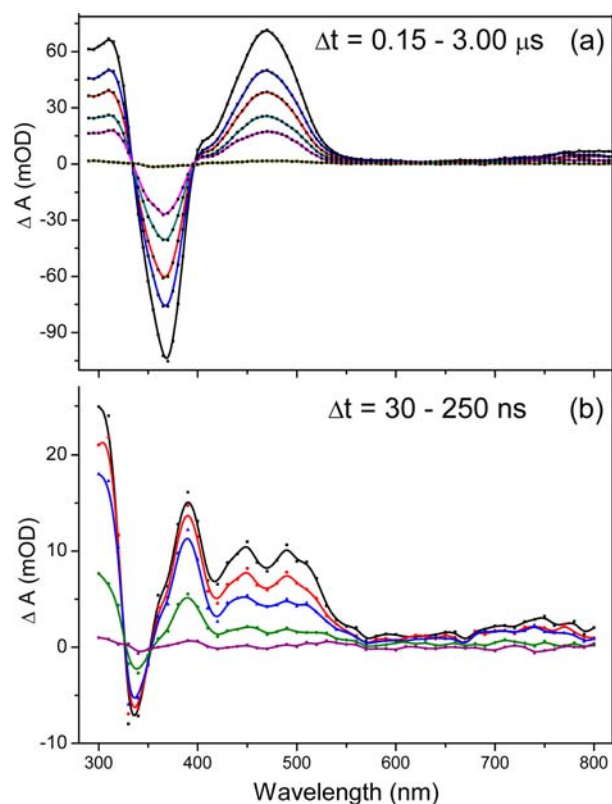
Figure 2. UV−vis TA spectra recorded at several time intervals (Δt) after 355 nm laser flash photolysis of (a) **1−N₂** in n-heptane ([N₂] = 8.8 mM), and (b) **2−N₂** in n-heptane ([N₂] = 8.8 mM). All data at 25 °C.

(between ca. 400 and 550 nm) and a much broader and weaker band in the NIR region (around 800 nm) were observed, together with an intense absorption in the UV region (<320 nm) and a bleach of the parent complex absorption at 370 nm ($1-N_2$) or 340 nm ($2-N_2$). The TA spectra for the $2-N_2$ complex were qualitatively similar to those for the $1-N_2$ complex. The visible and NIR transient absorption bands decayed together with single exponential kinetics, and the bleach recovered at the same rate. Kinetic traces recorded at the ground state absorption maxima revealed the complete recovery of $1-N_2$ and $2-N_2$, and UV−vis absorption spectra recorded before and after the experiment were identical, thus confirming that the photoreaction is fully reversible under these conditions (see Figure S4). Even when the experiment was performed under 400 Torr argon, in the absence of any additional N_2, the recovery of the $1-N_2$ transient bleach was 100% complete within 30 ms of excitation (see Figure S4).

The transient absorption spectra measured after 355 nm flash photolysis of $1-L$ and $2-L$ in *n*-heptane (L = H_2 and C_2H_4) are shown in Figures S5−S8 and are essentially identical to those measured for the nitrogen complexes. The transient absorption spectra of $1-N_2$ in toluene and THF are shown in Figures S9−S10. While the early time spectra in THF solution are similar to those in other solvents, the spectra recorded at longer time delays (ca. > 1 μs) show the appearance of a new band around 395 nm (i.e., the formation of $1-THF$, see the Discussion section below) that grows concomitantly with the decay of the 470 nm band, with an observed rate constant of 1.7×10^6 s^{-1} in the presence of 5.4 mM N_2. The decay of the 395 nm band has the same rate as the recovery of the ground state absorption at 370 nm. The photolysis of $1-L$ in THF under conditions of excess L was found to be reversible on the experimental time scale and was confirmed by comparing UV−vis spectra of the solution before and after transient experiments.

Kinetics of the Formation of Transient Species: Ultrafast Transient Absorption Spectroscopy. In an effort to identify the transient intermediate that absorbs at 470 and 800 nm, we performed a transient absorption experiment with $1-N_2$ in *n*-heptane in the presence of ∼9 mM N_2 on the femtosecond time scale with an apparatus that has an instrument response time of ∼400 fs. Since it has previously been shown that solvent molecules can take as long as a few picoseconds to bind to photogenerated coordinatively unsaturated metal centers,[14] we should observe the initial formation of a "naked" (PCP)Rh fragment followed by its solvation by a heptane molecule, if such a solvated species forms during the reaction. Interestingly, we found that the 470 and 800 nm transient bands are formed instantaneously (within the instrument response time), together with a much weaker, broad absorption band centered at 680 nm (Figure S12−S14). The 680 nm band then rapidly decays to 15% of its initial intensity with a lifetime of τ_{decay} = 1.04 ps (Figure S14), while the 470 and 800 nm bands remain stable for the 3 ns duration of the ultrafast experiment, with no other transient absorption features being observed. These data suggest that the 470 and 800 nm transient bands may be due to a long-lived coordinatively unsaturated (PCP)Rh^I fragment **1** rather than a solvent complex $1-$solvent. The 680 nm band may be due to a vibrationally "hot" state that cools on the 1 ps time scale.

Kinetics of Ligand Binding. After photoexcitation of $1-L$ or $2-L$, the observed rate of decay of the 470 nm transient band was monitored as a function of dissolved L concentration.

In the case of $1-L$ a plot of k_{obs} versus [L] yielded a straight line with a slope, equal to the second-order rate constant for reaction of the photogenerated "(PCP)Rh" fragment with L ($k_{470-slope}$), and an intercept ($k_{470-int}$) (Figure 3).
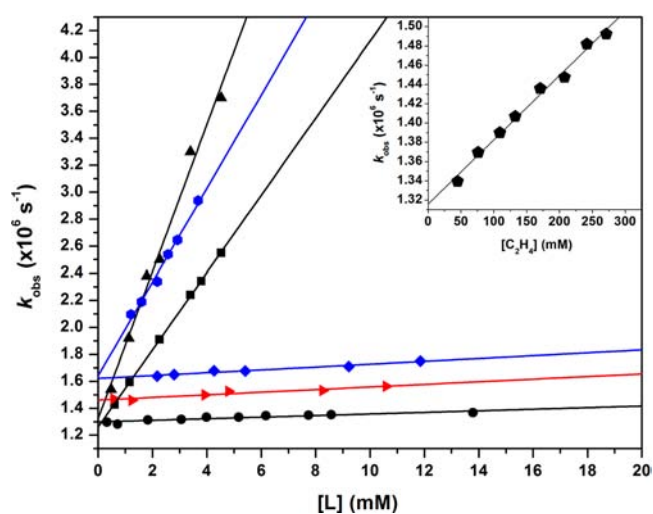

Figure 3. Plots of observed rate of decay (k_{obs}) versus concentration of L ([L]) for the 470 nm transient absorption band generated after 355 nm laser flash photolysis of $1-L$ (L = N_2, H_2, D_2 or C_2H_4) in *n*-heptane (black), toluene (red) and THF (blue) at 25 °C. C_2H_4 data are shown inset due to the much higher solubility of C_2H_4 than the other gases. ● (*n*-heptane, L = N_2), ▲ (*n*-heptane, L = H_2), ■ (*n*-heptane, L = D_2), ⬟ (*n*-heptane, L = C_2H_4), red triangle (toluene, L = N_2), blue diamond (THF, L = N_2), blue hexagon (THF, L = H_2).

The rate constants derived from the slope and intercept of the decay of the 470 nm band are summarized in Table 3 for

Table 3. Rate Constants Derived from the Slopes and Intercepts of Plots of the Observed Rate of Decay[a]

L	solvent	TA band (nm)	slope (M^{-1} s^{-1})	intercept (s^{-1})
N_2	*n*-heptane	470	4.0×10^6	1.3×10^6
H_2	*n*-heptane	470	5.5×10^8	1.3×10^6
D_2	*n*-heptane	470	2.9×10^8	1.3×10^6
C_2H_4	*n*-heptane	470	6.7×10^5	1.3×10^6
N_2	toluene	470	9.7×10^6	1.5×10^6
N_2	THF	470	1.1×10^7	1.6×10^6
H_2	THF	470	3.5×10^8	1.6×10^6
N_2	THF	395	4.7×10^6	0
H_2	THF	395	1.1×10^7	0

[a]k_{obs} versus [L] for the 470 and 395 nm transient absorption bands that are generated after 355 nm laser flash photolysis of $1-L$ (L = N_2, H_2, D_2, and C_2H_4) in *n*-heptane, toluene, and THF at 25 °C. All data have a ±10% instrumental error.

different incoming L and solvents. The second-order rate constant derived from the slope is dependent on both the incoming ligand and solvent, while the intercept depends only weakly on the solvent used. The rate constant derived from the slope indicates a normal KIE of 1.9 for the H_2/D_2 binding process.[90,91] The plots for the decay of the 395 nm transient band observed in THF as a function of L (Figure 4) had zero intercept, and the slopes are reported in Table 3.

The observed rate of decay of the 470 nm transient band after photoexcitation of $2-L$ is different from that of $1-L$. The decay of the transient absorption bands occurs on a shorter
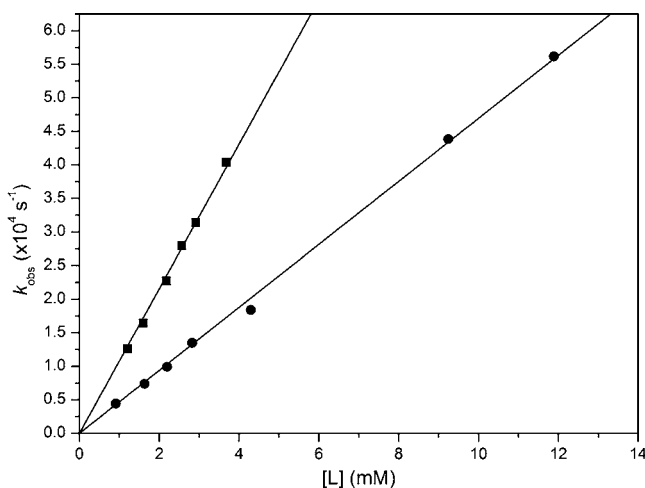
Figure 4. Plots of observed rate of decay (k_{obs}) versus concentration of L ([L]) for the 395 nm transient absorption band that is generated after 355 nm laser flash photolysis of **1−L** (L = N_2 or H_2) in THF at 25 °C. ● (L = N_2), ■ (L = H_2).

time scale than for **1−L** (ca. 5 times faster for L = N_2 and H_2, and ca. 14 times faster for L = C_2H_4). The observed rate constant of decay of the high-energy transient absorption band was plotted as a function of [L] (Figure 5). For L = N_2 and H_2
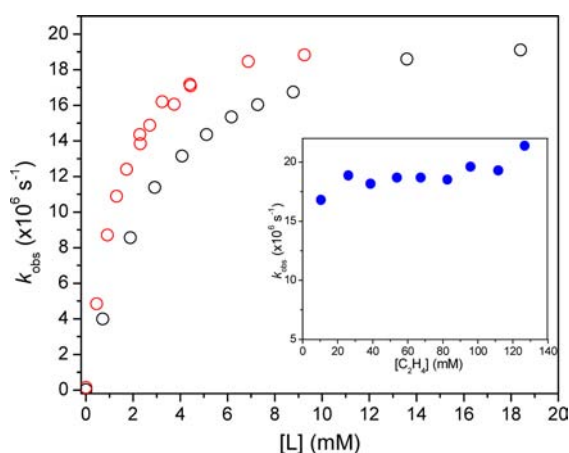

Figure 5. Plots of k_{obs} vs [L] for the decay of the visible transient absorption band generated after photoexcitation of **2−L**, L = N_2 (black) and H_2 (red) in *n*-heptane at 25 °C. C_2H_4 data are shown in the inset.

these plots are nonlinear, displaying saturation kinetics behavior, with k_{obs} increasing with [L], and then reaching a limiting value at [N_2] = 20 mM and [H_2] = 10 mM. It should be noted that the intercepts of these plots are essentially zero. Over the range of [C_2H_4] measured, the plot is approximately linear. However, it is difficult to operate below ca. 10 mM of C_2H_4 due to its high solubility in *n*-heptane, and therefore we

were likely observing the same limiting value of k_{obs} with L = C_2H_4 that we observed for L = H_2 and N_2 at [L] ≥ 10 and 20 mM, respectively. Double-reciprocal plots of $1/k_{obs}$ versus $1/$[L] for L = N_2 and H_2 were linear (Figure S11), indicating saturation kinetics. A linear fit of the reciprocal plots of $1/k_{obs}$ versus $1/$[L] resulted in 1.5×10^{-10} M s as a slope and 4.0×10^{-8} s as an intercept for **2−N₂**, and 7.5×10^{-11} M s as a slope and 4.0×10^{-8} s as an intercept for **2−H₂**.

The observation of nonlinear saturation kinetics and linear plots of $1/k_{obs}$ versus $1/$[L] (Figures 5 and S11, respectively) for **2−L** suggests a two-step scheme for the reaction of the photofragment generated in eq 7 with L to regenerate **2−L**, where the first step is reversible (eqs 8 and 9).

$$\textbf{2−L} \xrightarrow[-L]{h\nu} \textbf{2'} \tag{7}$$

$$\textbf{2'} \underset{k_{-1}}{\overset{k_1}{\rightleftharpoons}} \textbf{2} \tag{8}$$

$$\textbf{2} + \text{L} \xrightarrow{k_2} \textbf{2−L} \tag{9}$$

Applying the steady-state approximation to species **2**, it can be shown that a plot of $1/k_{obs}$ vs $1/$[L] should be linear, with an intercept equal to $1/k_1$ and a slope equal to k_{-1}/k_1k_2 (Figure S11). In order to extract the k_{-1} rate term from the slope, an estimation of k_2 must be made. In this case we estimate that k_2 is close or equal to the diffusion-controlled rate constant in *n*-heptane ($k_2 = k_{diff} = 1.7 \times 10^{10}$ M^{-1} s^{-1} for H_2 and 1.2×10^{10} M^{-1} s^{-1} for N_2).[92] This assumption is supported by fitting the initial slopes of the k_{obs} versus [L] plots in Figure 5, which reveals extremely high initial rate constants for the reaction of N_2 and H_2 with **2** (4.5×10^9 M^{-1} s^{-1} for N_2 and 8.3×10^9 M^{-1} s^{-1} for H_2).[93] A summary of the kinetic analysis for N_2 and H_2 binding to **2** is shown in Table 4.

Kinetics of the Ligand Binding at High Pressures: Activation Volume Studies. Measuring rate constants as a function of externally applied pressure (up to 2000 bar) can assist the formulation of a mechanism by allowing the volume of activation, $\Delta V^{\ddagger}$, for a process to be determined (eq 10).[94]

$$\left(\frac{\text{d ln } k}{\text{d}P}\right)_T = \frac{-\Delta V^{\ddagger}}{RT} \tag{10}$$

In general, for ligand substitution processes a positive $\Delta V^{\ddagger}$ indicates a dissociative transition state, and a negative $\Delta V^{\ddagger}$ implies an associative step, whereas a $\Delta V^{\ddagger}$ close to zero indicates an interchange mechanism, which has little or no pressure dependence. We have therefore monitored the rate of decay of the 470 nm transient absorption band as a function of external pressure for H_2 binding to **1** in *n*-heptane at 25 °C.

A series of pressure-dependent plots of k_{obs} versus [H_2] for the decay of the 470 nm transient absorption band after photoejection of H_2 from **1−H₂** in *n*-heptane (Figure S15) were constructed by transposing the data from several k_{obs} versus pressure plots at different H_2 concentrations. The slopes

Table 4. Kinetic Parameters for the Decay of the 430-nm Band Following Photoexcitation of 2−L in *n*-Heptane[a]

L	slope (M s)	intercept (s)	k_1 (s^{-1})	k_{-1} (s^{-1})	K_{eq} (k_1/k_{-1})
N_2	1.5×10^{-10}	4.0×10^{-8}	2.5×10^7	4.5×10^7	0.6 ± 0.1
H_2	7.5×10^{-11}	4.0×10^{-8}	2.5×10^7	3.2×10^7	0.8 ± 0.1

[a]Obtained from linear plots of $1/k_{obs}$ vs $1/$[L] ($k_2 \equiv k_{diff} = 1.7 \times 10^{10}$ M^{-1} s^{-1} and 1.2×10^{10} M^{-1} s^{-1} for H_2 and N_2, respectively). The initial error of 10% for both the slope and intercept will propagate to 17% in K_{eq} due to the calculations involved.

and intercepts from the plots in Figure S15 were then used to construct $\ln(k_{slope})$ and $\ln(k_{intercept})$ versus pressure plots (Figure 6). As can be seen in Figure 6, the intercept rate
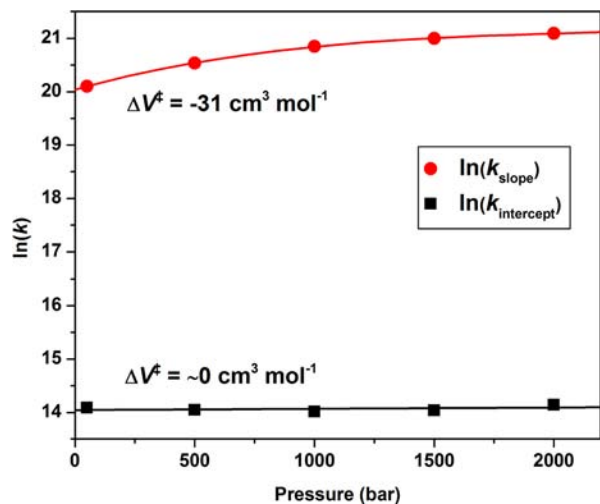

Figure 6. Plots of $\ln(k_{slope})$ and $\ln(k_{intercept})$ versus externally applied pressure, where k_{slope} and $k_{intercept}$ are the rate constants obtained from the slopes and intercepts of the graphs shown in Figure S15.

constant essentially has a zero pressure dependence, implying that the process associated with the intercept in our kinetic plots could have an interchange nature. However, the rate constant from the slope exhibits significant pressure dependence. The curvature of this plot is caused by the compressibility of the solvent, and the data were fitted to a polynomial expression to account for this.[94] Extracting the linear slope from the fit revealed an activation volume, $\Delta V^{\ddagger}$ of -31 cm^3 mol^{-1}, which is strongly negative and indicative of an associative mechanism for the binding of H$_2$ (and presumably the other incoming ligands under study) to the 470 nm absorbing transient species. Similar investigations of the pressure dependence of the slope and intercept rate constants

for N$_2$ and C$_2$H$_4$ binding were not undertaken since the changes in observed rate constant, k_{obs}, as a function of [N$_2$] and [C$_2$H$_4$] are much smaller than for H$_2$, making the high-pressure experiments less informative.

Theoretical Calculations. The gas-phase calculated 1−N$_2$ complex was found to share similar geometrical parameters with those in analogous (PCP)Rh complexes (Figure S16),[45,69] suggesting that the structure of the common (PCP)Rh framework is not sensitive to ligands such as N$_2$, H$_2$, and C$_2$H$_4$ in the ground state. Although the four ^{t}Bu groups provide a certain amount of steric bulk, it is clear that the Rh coordination cavity is sufficiently open that ligands at least as large as C$_2$H$_4$ can bind with ease (Figure S16). The square planar Rh center is also open to attack from above and below the (PCP)Rh coordination plane.[95]

We have also calculated the structures of the 3-coordinate 14-electron "naked" (PCP)Rh species, 1 (Figure 7a), and the 4-coordinate n-hexane and THF solvated complexes, 1−hexane and 1−THF. For 1, we were unable to locate a structure with strong internal agostic interactions from the four $tert$-butyl groups, even after repeating the calculation at the higher MP2(FC) level of theory, with the closest Rh···H interactions being 3.095 Å (Figure 7a). When we performed a DFT calculation on the saturated version of the complex, 2, a significant agostic interaction was located between the Rh center and the C−H bond of the central C atom in the PCP ligand backbone (Figure 7b, Rh−H 2.545 Å, Rh−C 2.068 Å). A similar agostic interaction was previously reported by Milstein in the 2−CO$_2$ complex.[68]

In order to further probe the nature of the intermediate species observed by transient absorption spectroscopy, we performed gas-phase TD-DFT calculations on three-coordinate 1 and four-coordinate 1−L complexes (L = n-hexane, THF, N$_2$, H$_2$, and C$_2$H$_4$) for comparison with the experimentally observed UV−vis and TA spectra. Although the calculated spectra are slightly blue-shifted, good agreement between the spectral features of the calculated and experimentally acquired UV−vis spectra of 1−N$_2$, 1−H$_2$, and 1−C$_2$H$_4$ was observed

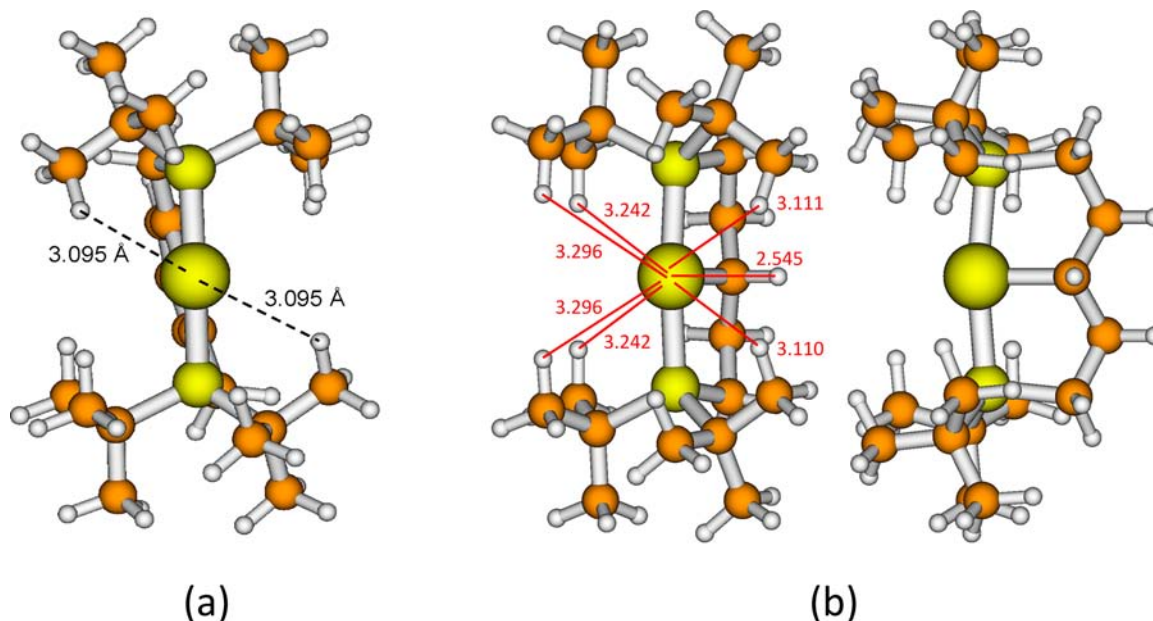**Figure 7.** (a) MP2(FC)-calculated structure of 1, and (b) DFT-calculated structure of agostically stabilized 2.

(see Figures S17−S19). Assignments of the calculated UV−vis transitions for **1−N₂** are provided in the SI (Figure S20 together with a list of assignments and discussion immediately following that figure). The computed UV−vis spectra of **1**, **1−hexane**, and O-coordinated **1−THF** are shown in Figure 8.
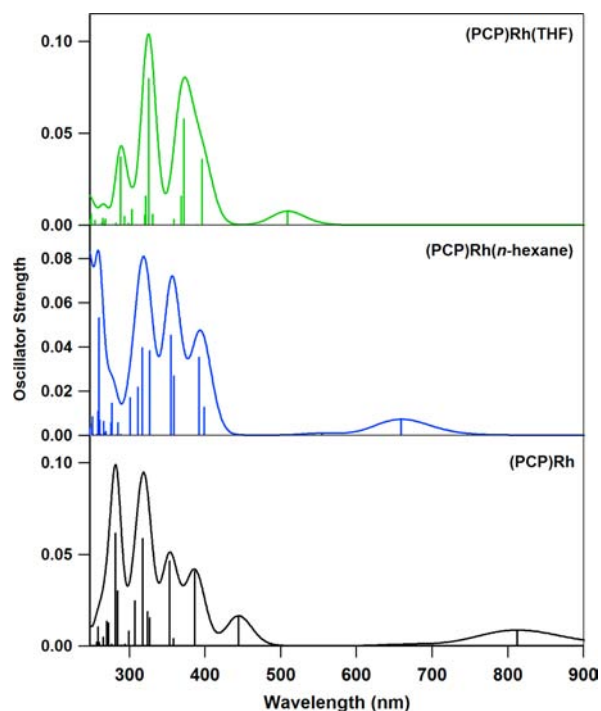

Figure 8. Gas-phase TD-DFT calculated UV−vis spectra of O-coordinated **1−THF**, **1−hexane**, and **1**. Vertical lines show the transitions, and the curves were generated by a multi-Gaussian function with bandwidths of 0.25 eV.

The hexane complex is predicted to have a weak absorption band at 660 nm, with much more intense overlapping bands at shorter wavelengths (below 400 nm), while the THF complex is calculated to exhibit a weak band at 509 nm, again with more intense overlapping bands below 400 nm. The calculated **1−THF** spectrum is similar to the UV−vis spectrum of the Rh^I species formed after Na/Hg reduction of **1−(H)(Cl)** in THF under vacuum (see Figure S2). In contrast, the coordinatively unsaturated, 3-coordinate (PCP)Rh fragment is predicted to have a reasonably intense band at 445 nm, a much broader, weak absorption at 813 nm, and more intense overlapping bands below 400 nm. It is noteworthy that no bands were predicted for the hexane or THF complexes at wavelengths longer than 660 nm. Despite the fact that they are slightly shifted, the 445 and 813 nm calculated bands of 3-coordinate (PCP)Rh are remarkably similar to the 470 and 800 nm bands that were observed by transient absorption spectroscopy immediately upon photoejection of L from the **1−L** complexes.

The bonding in the (PCP)Rh^I complexes is more complicated than might be expected. The d^8 Rh(I) center in pseudo-square-planar complexes (with the z-axis perpendicular to the P−Rh−P plane) has pairs of electrons in the lowest (degenerate) d$_{yz}$ and d$_{xz}$ (dπ) orbitals, another pair in the d$_{z^2}$ orbital, and still another pair in the d$_{xy}$ orbital, with the highest lying d$_{x^2−y^2}$ orbital unoccupied. While one might imagine a ligand L on the x-axis to donate a lone pair of electrons in a σ orbital to the unoccupied d$_{x^2−y^2}$ orbital, which has a lobe
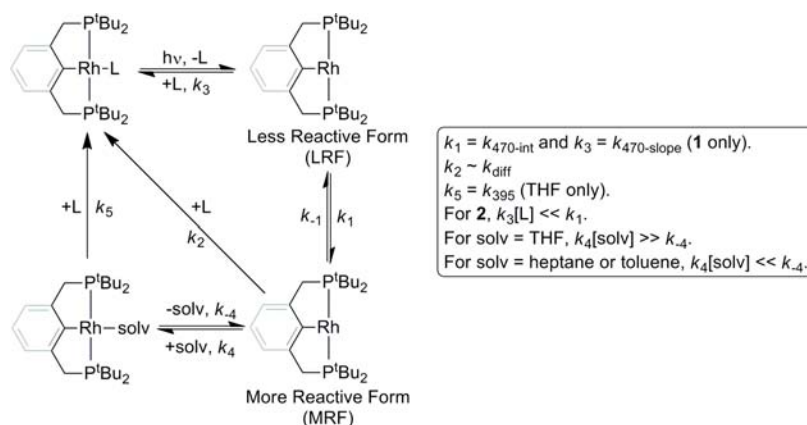
pointing directly at the incoming ligand along the x-axis, the situation is more complicated. Indeed, the donation of the lone pair on N₂ in an end-on (η^1) attack, or by H₂ in a sideways (η^2) attack almost perpendicular to the P−Rh−P plane and parallel to the z-axis, stabilizes the bonding σ orbital to HOMO − 12 (Figures S21 and S22). The corresponding anitbonding orbital (HOMO − 7) is also doubly occupied. In the case of N₂, the pair of electrons in the d$_{xy}$ orbital is donated into the vacant in-plane N₂ π_y* orbital (HOMO − 3) and the pair in the d$_{xz}$ orbital is donated into the out-of-plane N₂ π_z* orbital, forming π bonds between the Rh and near N atom. The N−N bond in these two orbitals is π-antibonding in character (Figure S21). In the case of H₂, the pair of electrons in the d$_{yz}$ orbital (a π orbital with nodes in the xy and xz planes) is donated (HOMO − 5) to the unoccupied σ* orbital between two H atoms (with a node in the xy plane) to form symmetry-breaking "wrap-around" σ-like bonds between the Rh atom and the two H atoms (in which the xz nodal plane of the orbital rotates into the xy plane in going from the Rh center to the two H atoms). Participation of oppositely phased orbitals on the two P atoms is also involved. HOMO − 1 also forms σ bonds between Rh and the two H atoms through the interaction of the Rh d$_{xz}$ and H₂ σ* orbitals, while decreasing the strength of the σ bond between the two H atoms (Figure S22). In both cases, the HOMO is the lone pair in the d$_{z^2}$ orbital. The bonding in the ethylene complex is similar to that in the H₂ complex except it involves the π and π* orbitals between the two C atoms of the adduct (that lie roughly parallel to the z axis but slightly rotated about the y axis) interacting with the Rh d$_{x^2−y^2}$ and d$_{xz}$ orbitals (Figure S23).

■ DISCUSSION

Thermodynamics of Small Molecule and Solvent Binding. The relative binding affinities of L = H₂, N₂, and C₂H₄ to **1** were measured by high-pressure equilibrium NMR methods. We found that H₂ binding to **1** is more favorable than N₂ binding ($\Delta G°_{298} = −0.71$ kcal mol$^{−1}$ for L = H₂ in eq 5), while C₂H₄ binding is less favorable than dinitrogen binding ($\Delta G°_{298} = +1.08$ kcal mol$^{−1}$), Table 2. This may be partially due to the different sizes of the incoming ligands, although differences in the electronic bonding properties of the ligands will also play a role. Milstein and co-workers found a similar trend in binding free energies for **2**.[68] These trends differ from those of the related mer,trans-W(CO)₃(PCy₃)₂(N₂) system, in which the binding of H₂ and C₂H₄ are both less favorable than N₂ binding by $\Delta G°_{298} = +0.2$ and $+2.3$ kcal mol$^{−1}$, respectively.[15] However, this is not surprising given that the tungsten complex fundamentally differs from the current rhodium system in that it possesses an octahedral configuration of ligands and thus a very different bonding environment and molecular orbital configuration.

Kinetics of Small Molecule Binding and Mechanistic Interpretation. Photoexcitation of **1−L** or **2−L** leads to dissociation of L, yielding the coordinatively unsaturated species **1** or **2** and a free ligand L. In the TA spectra of **1−L** and **2−L** in n-heptane and toluene (**1−L** only), the transient intermediate observed immediately after photoejection of L possesses bands at 470 and 800 nm for **1**, and at 300−500 and 750 nm for **2**. Despite the relatively long observed lifetime of this species ($\tau = 50−800$ ns, depending on which gas, L, was used and its concentration), there is convincing evidence from our experiments to suggest that it does not possess any significant Rh−solvent interaction, as follows. (i) Apart from a

Scheme 2. Proposed Mechanism for the Binding of L to the Photofragment Generated upon Photoejection of L from 1−L (L = N₂, H₂, D₂, or C₂H₄) or 2−L (L = N₂, H₂ or C₂H₄) in *n*-Heptane, Toluene, and THF[a]

$k_1 = k_{470\text{-int}}$ and $k_3 = k_{470\text{-slope}}$ (**1** only).
$k_2 \sim k_{\text{diff}}$
$k_5 = k_{395}$ (THF only).
For **2**, $k_3[\text{L}] \ll k_1$.
For solv = THF, $k_4[\text{solv}] \gg k_{-4}$.
For solv = heptane or toluene, $k_4[\text{solv}] \ll k_{-4}$.

[a]The PCP ligand backbone is shown in gray/black for **1** and in black only for **2**. The values of k_1−k_5 and the predominant reaction pathways depend on the nature of the PCP ligand, solvent, and L, as shown in the scheme and in Tables 3 and 4. k_{diff} = diffusion-controlled rate constant.

slight blue shifting of the bands, our TD-DFT calculated UV−vis spectrum of three-coordinate **1** (Figure 8) is a good match to the experimentally observed femtosecond and nanosecond TA spectra of **1**. In contrast, the calculated spectra of the **1**−hexane and **1**−THF solvent complexes are a poor match, particularly due to the complete absence of any calculated bands near 800 nm. (ii) The position of the 470 nm band observed in the ns-TA spectra of **1** was independent of the nature of the solvent. If this band were due to a solvent complex, we would expect the band to shift, especially in the more coordinating solvent, THF (cf. Figures 2 and S10, and Table 1; **1**−THF at 386, 486 nm vs **1** at 470, 800 nm TA bands). Shifts of >100 nm for the visible absorption bands of coordinatively unsaturated transition metal complexes that are weakly bound to σ-donor ligands of different donating ability have previously been observed in cryogenic matrices[96] and in room temperature solutions.[97] Our TD-DFT calculations also predicted a +151 nm shift of the visible band from 509 nm for **1**−THF to 660 nm for **1**−hexane (Figure 8), in which the hexane binding enthalpy is computed to be 6.8 kcal mol⁻¹ weaker than that of THF. (iii) The second-order rate constants for N₂ and H₂ binding derived from the slopes of the k_{obs} vs [L] plots for the decay of the 470 nm band of **1** are much greater (up to a factor of 625) than those for analogous reactions of N₂ and H₂ with solvated species such as CpMn(CO)₂(*n*-heptane)[98] and W(CO)₅(*n*-heptane),[99] which require a bound solvent molecule to be replaced by N₂ or H₂. Similarly, the binding of N₂ and H₂ to **1** is 13 and 183 times faster, respectively, than for binding to *mer,trans*-W(CO)₃(PCy₃)₂,[15] which possesses a strong internal agostic interaction that must be broken for binding to occur. (iv) The large negative value of $\Delta V^{\ddagger}$ (−31 cm³ mol⁻¹) for the second-order process associated with the decay of the 470 nm transient band for H₂ binding to **1** in *n*-heptane indicates a strongly associative transition state for the addition of L, which would be expected for binding to a nonsolvated species. During this process, H₂ almost completely disappears from the bulk solution as it binds to the vacant coordination site on **1**, causing a large volume collapse on going to the transition state. It should be noted however, that binding to an essentially square-planar (PCP)Rh(solvent) species could also be associative, but typically with a less negative value of $\Delta V^{\ddagger} \sim -10$ cm³ mol⁻¹.[100] (v) Femtosecond TA spectroscopy

in *n*-heptane showed that the 470 and 800 nm absorption bands of **1** are formed within the ∼400 fs response time of the instrument. If these bands were due to a solvent complex, their formation may be expected to take longer (e.g., a few picoseconds).[14]

The preceding arguments suggest that the transient species observed immediately after photoejection of L from **1**−L, and presumably also from **2**−L, does not possess a significant Rh−solvent bond, and that if any Rh···solvent interaction exists it must be extremely weak. Certainly, the very strong Rh−C bond *trans* to the vacant coordination site in **1** and **2** will serve to weaken any interaction with the solvent in this position. Despite the absence of apparent interaction with solvent, the kinetic evolution of **1** and **2** appears to be complex. For example, the conversion of **2** to **2**−L proceeds via a precursor, **2′**, which exists in equilibrium with **2** (see eqs 8 and 9). The results of a kinetic analysis of N₂ and H₂ binding to **2** (Table 4) indicate that, within experimental error, the equilibrium constant between **2′** and **2** is independent of the nature of L. The difference in observed kinetic behavior for the binding of N₂ and H₂ to **2** is thus solely due to the different binding rate constants, k_2 for N₂ and H₂. Therefore, we propose the following general reaction scheme to explain the reactivity of **2** with H₂ and N₂ ligands in *n*-heptane (Scheme 2, except for the k_4 and k_5 pathways).[101]

In the TA experiments, the less-reactive form (LRF), **2′**, is observed immediately upon photoejection of L from **2**−L, with absorption bands at 300−550 and 750 nm. This is in equilibrium with another species, the more-reactive form (MRF), **2**, which reacts with the incoming ligand, L, to regenerate **2**−L with a diffusion-controlled rate constant. We assign the LRF and MRF as different conformers of three-coordinate **2**, exhibiting different reactivity toward L. Although we calculated an agostic structure for **2** (Figure 7b), and a similar agostic interaction with the central C−H bond of the PCP ligand has previously been reported by Milstein and co-workers in the CO₂ complex, **2**−CO₂,[68] we do not have any direct evidence that the LRF is an agostically stabilized species and therefore cannot make a definitive conclusion about its precise structural form. The equilibrium between the LRF and MRF slightly favors the LRF, which is consistent with the LRF being more stable and its lack of reactivity toward incoming

ligands. However, once it is converted into the MRF, which must have a more open molecular configuration, it is subject to attack by incoming ligands at a rate constant, k_2 that is diffusion-controlled. Kinetic simulations for both the N_2 and H_2 binding using the IBM Chemical Kinetics Simulator,[102] in which k_2 was set to the diffusion-controlled rate constants stated in the caption to Table 4, and k_1 and k_{-1} were set to the rate constants shown in Table 4, provide an excellent fit to the experimental data (see Figure S24). Attempts to set k_2 to lower than a diffusion-controlled rate constant did not provide a satisfactory fit to the data.

In contrast to the binding of L to **2**, nonlinear saturation kinetics were not observed (Figure 3) for the decay of the 470 nm band of **1'** (which corresponds to the LRF of **1** in Scheme 2),[103] even at very low N_2 concentrations (down to 0.20 mM).[103] This implies that for **1'**, the first step involving conversion of **1'** to **1** (LRF → MRF), is irreversible, or an equilibrium that is heavily shifted toward the MRF. Therefore, our proposed mechanism for the binding of L to **1** is similar to that for binding to **2**, but irreversible in the first step (Scheme 2, $k_{-1} \approx$ 0). Again, since we do not have direct evidence for the identities of the LRF and MRF, we conclude that they are different conformers of **1** that exhibit different reactivity toward incoming ligands, L, without speculating further about their specific structures. Since the LRF → MRF reaction is irreversible, this implies that **1'** is a higher-energy, metastable species that must overcome an energy barrier to generate the more reactive **1**. Such a high-energy configuration of **1'** may be accessible due to the excess vibrational energy left over after photocleavage of the **1**−L bond. Our DFT and MP2(FC) calculations failed to locate any significant agostic interactions for **1**, so it is unlikely that agostic stabilization is involved. However, there are other possibilities for the identity of **1'** (and **2'**) including (i) a species in which a solvent molecule is partially blocking the coordination cavity, thus hindering access by L, (ii) a different spin state (e.g., a triplet) that is less reactive toward L, and (iii) a species resulting from reaction with a weakly binding impurity, although this is unlikely under the described experimental conditions (see below).

Arguably, the intercepts of k_{obs} versus [L] plots may contain contributions from one or more competing side reactions, such as reaction with impurities. However, we note that the magnitudes of the intercepts in Figure 3 are significant (on the order of 10^6 s^{-1}) when compared to similar experiments previously performed in our laboratory in the same solvents purified by the same techniques (in which intercepts on the order of 10^2 to 10^3 s^{-1} were obtained).[15] Furthermore, we reproducibly observed very similar intercepts ($\sim 10^6$ s^{-1}) in the three different solvents investigated (Figure 3), using different batches of each solvent and different samples of **1**−L, and we always observed complete photoreversibilty of the solutions, based on UV−vis spectra recorded before and after laser excitation (see Figure S4). Therefore, we believe that reaction with impurities is not an important factor in the current experiments. The intercepts in Figure 3 show a very weak trend of solvent dependence, while being independent of L in a given solvent. It is therefore likely that these intercepts represent the observed rate constant for the transformation of the LRF, **1'** into the MRF, **1** (Scheme 2). This assignment agrees with the zero activation volume that we found for the $k_{470\text{-int}}$ intercept rate constant for H_2 binding to **1** in *n*-heptane, since the transformation is not expected to involve significant volume changes.

In addition to the L-independent pathway described above, the LRF, **1'**, reacts directly with L with second-order rate constants corresponding to the slopes in Figure 3 (see also eq 11). For this pathway, a large negative activation volume was found (L = H_2) indicating an associative transition state. This pathway is not significant in the binding of L to **2**, presumably due to the more flexible nature of the saturated PCP ligand framework allowing **2'** to adopt a more stable conformation that is less reactive compared to **1'**. The rate constants for the binding of L to **1'** vary by almost 3 orders of magnitude, depending on the nature of L and the solvent, increasing in the order L = C_2H_4 < N_2 < D_2 < H_2 (Table 3). Such a large variation in rate constant suggests that steric hindrance at the Rh center influences the binding kinetics, although differences in the electronic bonding properties of the ligands, together with solvent viscosity, dielectric constant, and differences in the solvation energies of the small ligands, L, will also likely play a role. We have performed kinetic simulations based on the proposed mechanism, and these provide an excellent fit to the experimental data (Figure S25). We note that rate constants ranging from 10^8 to 10^{10} M^{-1} s^{-1} for the reaction of the MRF, **1**, with N_2 allowed us to accurately simulate the experimental data.

$$1' + L \overset{k_3}{\to} 1-L \tag{11}$$

In the case of strongly coordinating solvents, such as THF, it was found that the MRF, **1**, will also react with a solvent molecule to form a solvent-bound species, **1−Solv** (Scheme 2). In the TA spectra of **1−L** in THF, a transient band at 395 nm grows in from the 470/800 nm bands (see inset in Figure S10). This is very similar to the 386 nm band of **1−THF** prepared by Na/Hg reduction of **1−(H)(Cl)**, see Figure S2. The intercept of the plot of k_{obs} versus [L] for the decay of the 470 nm band (1.6×10^6 s^{-1}) still represents the observed rate constant for the rearrangement of the LRF, **1'**, to the MRF, **1**. The direct reaction of L with **1'** is also still operative, with a rate constant of $k_{470\text{-slope}}$ (see Table 3). While the direct measurement of the rate of reaction between **1** and THF was not possible due to the LRF → MRF transformation being the rate-determining step, this rate can be estimated from kinetic simulations based on the proposed mechanism and experimental data. Kinetic simulations for N_2 binding to **1** in THF according to the proposed mechanism provide an excellent fit to the experimental data, reproducing the k_{obs} versus [L] plots (Figures S26−27) and the experimental kinetic decay traces. In these simulations, a lower limit for the second-order rate constant for the reaction of **1** with THF was found to be $\sim 10^7$ M^{-1} s^{-1}. This rate constant is significantly lower than the rate constant for the reaction between **1** and gas molecules, which was estimated to be close to the diffusion-controlled limit. This is consistent with the significant difference in the size of the incoming solvent molecule compared to a gas molecule (N_2, H_2, etc). After the formation of the solvent bound species **1−THF**, it slowly reacts with L to yield **1−L** and a free solvent molecule with a rate constant of k_{395} (see Table 3).

The overall proposed mechanism for the binding of L (L = N_2, H_2, D_2, and C_2H_4) to the photofragment generated upon photoejection of L from **1−L** and **2−L** in *n*-heptane, toluene, and THF is shown in Scheme 2. The values of the rate constants, k_1−k_5, and the predominant reaction pathways depend on the nature of the complex (**1−L** or **2−L**), and on the identity of the solvent and ligand, L as discussed above (see

inset in Scheme 2, and Tables 3 and 4). In both cases, the two unsolvated intermediate species that are observed, **1′** (**2′**) and **1** (**2**), are assumed to be different conformers that exhibit different reactivity toward L. While the identities of these intermediate species cannot be conclusively determined at this time, the proposed mechanism is the only one of many that were considered that fits the experimentally observed kinetic data well. More detailed experiments would be required in order to make a more definitive assignment of the intermediates.

■ CONCLUSION

In summary, we have conducted equilibrium and kinetic studies for the binding of N_2, H_2, D_2, and C_2H_4 to the $(PCP)Rh^I$ complexes, **1** and **2**, by NMR spectroscopy and transient spectroscopic techniques, including TRIR and UV−vis transient absorption under both ambient and high-pressure conditions. The equilibrium studies revealed that the relative free energies of binding increase in the order $C_2H_4 < N_2 < H_2$. On the basis of our kinetic measurements and kinetic modeling, we have proposed mechanistic pathways for the binding of L to the intermediates generated upon photoejection of L from **1−L** and **2−L**. In both cases, the initial species formed after photoejection of L is unsolvated **1′** or **2′**, which is the so-called less-reactive form. **2′** is in equilibrium with a more-reactive form, **2**, which reacts with L to regenerate **2−L** at diffusion-controlled rates. These different forms are assumed to be different conformers of the (PCP)Rh fragment that exhibit different reactivity toward L. For **1**, we propose a similar mechanism but with the transformation of **1′** to **1** proceeding irreversibly. However, a parallel reaction pathway is also in operation for **1′**, involving its direct reaction with L with a second-order rate constant that is strongly influenced by the size of the incoming ligand, L, varying by almost 3 orders of magnitude. Solvent binding to **1** could only be observed in THF by the formation of a second transient band at 395 nm. The large variation in binding rate constants, and the fact that long-lived unsolvated species ($\tau = 50−800$ ns, depending on L and its concentration in solution) are the primary transients observed in the binding of L to **1** and **2**, suggests that steric hindrance at the Rh center influences the binding kinetics in this family of (PCP)Rh complexes. The nature of the solvent also plays a significant role in determining the mechanism of binding, as does the structure of the PCP ligand, and this may have implications for the control of mechanisms of small molecule activation with these and related complexes. Future investigations will focus on the use of different solvents of varying donating ability and steric bulk to more fully determine the effect of solvent on reactivity. A more detailed investigation of **2−L**, including pressure dependence studies, will also be conducted in different solvents.

■ ASSOCIATED CONTENT

Ⓢ Supporting Information

Full ref 76, additional experimental details, UV−vis, TRIR, and TA spectra, TD-DFT calculated UV−vis spectra, DFT-calculated geometrical parameters, Cartesian coordinates and energies of all species calculated by DFT, kinetic simulation results. This material is available free of charge via the Internet at http://pubs.acs.org.

■ AUTHOR INFORMATION

Corresponding Author

*E-mail: dcgrills@bnl.gov (D.C.G.), dmitriyp@bnl.gov (D.E.P.), fujita@bnl.gov (E.F.).

Present Addresses

§General Electric Global Research, One Research Circle, Niskayuna, New York 12309, United States.
∥Division of Chemical and Life Sciences and Engineering and KAUST Catalysis Center, King Abdullah University of Science and Technology (KAUST), Thuwal, 23955−6900, Saudi Arabia.

Notes

The authors declare no competing financial interest.

■ REFERENCES

(1) Brown, C. E.; Ishikawa, Y.; Hackett, P. A.; Rayner, D. M. *J. Am. Chem. Soc.* **1990**, *112*, 2530.
(2) Grills, D. C.; Huang, K.-W.; Muckerman, J. T.; Fujita, E. *Coord. Chem. Rev.* **2006**, *250*, 1681.
(3) Ishikawa, Y.; Brown, C. E.; Hackett, P. A.; Rayner, D. M. *Chem. Phys. Lett.* **1988**, *150*, 506.
(4) Wells, J. R.; Weitz, E. *J. Am. Chem. Soc.* **1992**, *114*, 2783.
(5) Anfinrud, P. A.; Han, C.-H.; Lian, T.; Hochstrasser, R. M. *J. Phys. Chem.* **1991**, *95*, 574.
(6) Dobson, G. R.; Hodges, P. M.; Healy, M. A.; Poliakoff, M.; Turner, J. J.; Firth, S.; Asali, K. J. *J. Am. Chem. Soc.* **1987**, *109*, 4218.
(7) Joly, A. G.; Nelson, K. A. *J. Phys. Chem.* **1989**, *93*, 2876.
(8) Klassen, J. K.; Selke, M.; Sorensen, A. A.; Yang, G. K. *J. Am. Chem. Soc.* **1990**, *112*, 1267.
(9) Lee, M.; Harris, C. B. *J. Am. Chem. Soc.* **1989**, *111*, 8963.
(10) Simon, J. D.; Xie, X. *J. Phys. Chem.* **1986**, *90*, 6751.
(11) Simpson, M. B.; Poliakoff, M.; Turner, J. J.; Maier, W. B., II; McLaughlin, J. G. *J. Chem. Soc., Chem. Commun.* **1983**, 1355.
(12) Wang, L.; Zhu, X.; Spears, K. G. *J. Phys. Chem.* **1989**, *93*, 2.
(13) Xie, X. L.; Simon, J. D. *J. Am. Chem. Soc.* **1990**, *112*, 1130.
(14) Joly, A. G.; Nelson, K. A. *Chem. Phys.* **1991**, *152*, 69.
(15) Grills, D. C.; van Eldik, R.; Muckerman, J. T.; Fujita, E. *J. Am. Chem. Soc.* **2006**, *128*, 15728.
(16) Wasserman, H. J.; Kubas, G. J.; Ryan, R. R. *J. Am. Chem. Soc.* **1986**, *108*, 2294.
(17) Hall, C.; Perutz, R. N. *Chem. Rev.* **1996**, *96*, 3125.
(18) Bengali, A. A.; Schultz, R. H.; Moore, C. B.; Bergman, R. G. *J. Am. Chem. Soc.* **1994**, *116*, 9585.
(19) Grills, D. C.; Sun, X. Z.; Childs, G. I.; George, M. W. *J. Phys. Chem. A* **2000**, *104*, 4300.
(20) Schultz, R. H.; Bengali, A. A.; Tauber, M. J.; Weiller, B. H.; Wasserman, E. P.; Kyle, K. R.; Moore, C. B.; Bergman, R. G. *J. Am. Chem. Soc.* **1994**, *116*, 7369.
(21) Simon, J. D.; Peters, K. S. *Chem. Phys. Lett.* **1983**, *98*, 53.
(22) Bengali, A. A.; Bergman, R. G.; Moore, C. B. *J. Am. Chem. Soc.* **1995**, *117*, 3879.

(23) Muckerman, J. T.; Fujita, E.; Hoff, C. D.; Kubas, G. J. *J. Phys. Chem. B* **2007**, *111*, 6815.

(24) Montag, M.; Efremenko, I.; Cohen, R.; Leitus, G.; Shimon, L. J. W.; Posner-Diskin, Y.; Ben-David, Y.; Martin, J. M. L.; Milstein, D. *Chem.—Eur. J.* **2008**, *14*, 8183.

(25) Siegbahn, P. E. M. *J. Am. Chem. Soc.* **1996**, *118*, 1487.

(26) Siegbahn, P. E. M.; Svensson, M. *J. Am. Chem. Soc.* **1994**, *116*, 10124.

(27) Ingleson, M.; Fan, H.; Pink, M.; Tomaszewski, J.; Caulton, K. G. *J. Am. Chem. Soc.* **2006**, *128*, 1804.

(28) Rimmer, R. D.; Grills, D. C.; Fan, H.; Ford, P. C.; Caulton, K. G. *J. Am. Chem. Soc.* **2007**, *129*, 15430.

(29) Portius, P.; Yang, J. X.; Sun, X. Z.; Grills, D. C.; Matousek, P.; Parker, A. W.; Towrie, M.; George, M. W. *J. Am. Chem. Soc.* **2004**, *126*, 10713.

(30) Macgregor, S. A.; Eisenstein, O.; Whittlesey, M. K.; Perutz, R. N. *J. Chem. Soc., Dalton Trans.* **1998**, 291.

(31) Osman, R.; Perutz, R. N.; Rooney, A. D.; Langley, A. J. *J. Phys. Chem.* **1994**, *98*, 3562.

(32) Nicasio, M. C.; Perutz, R. N.; Tekkaya, A. *Organometallics* **1998**, *17*, 5557.

(33) Osman, R.; Pattison, D. I.; Perutz, R. N.; Bianchini, C.; Casares, J. A.; Peruzzini, M. *J. Am. Chem. Soc.* **1997**, *119*, 8459.

(34) Cronin, L.; Nicasio, M. C.; Perutz, R. N.; Peters, R. G.; Roddick, D. M.; Whittlesey, M. K. *J. Am. Chem. Soc.* **1995**, *117*, 10047.

(35) Hall, C.; Jones, W. D.; Mawby, R. J.; Osman, R.; Perutz, R. N.; Whittlesey, M. K. *J. Am. Chem. Soc.* **1992**, *114*, 7425.

(36) Fujita, E.; Creutz, C.; Sutin, N.; Szalda, D. J. *J. Am. Chem. Soc.* **1991**, *113*, 343.

(37) Fujita, E.; Creutz, C.; Sutin, N.; Brunschwig, B. S. *Inorg. Chem.* **1993**, *32*, 2657.

(38) Ogata, T.; Yanagida, S.; Brunschwig, B. S.; Fujita, E. *J. Am. Chem. Soc.* **1995**, *117*, 6708.

(39) Fujita, E.; Furenlid, L. R.; Renner, M. W. *J. Am. Chem. Soc.* **1997**, *119*, 4549.

(40) Fujita, E.; van Eldik, R. *Inorg. Chem.* **1998**, *37*, 360.

(41) Fujita, E.; Wishart, J. F.; van Eldik, R. *Inorg. Chem.* **2002**, *41*, 1579.

(42) Yan, S. G.; Brunschwig, B. S.; Creutz, C.; Fujita, E.; Sutin, N. *J. Am. Chem. Soc.* **1998**, *120*, 10553.

(43) Fujita, E.; Brunschwig, B. S.; Creutz, C.; Muckerman, J. T.; Sutin, N.; Szalda, D.; van Eldik, R. *Inorg. Chem.* **2006**, *45*, 1595.

(44) Hayashi, Y.; Kita, S.; Brunschwig, B. S.; Fujita, E. *J. Am. Chem. Soc.* **2003**, *125*, 11976.

(45) Huang, K.-W.; Han, J. H.; Musgrave, C. B.; Fujita, E. *Organometallics* **2007**, *26*, 508.

(46) Polyansky, D. E.; Cabelli, D.; Muckerman, J. T.; Fukushima, T.; Tanaka, K.; Fujita, E. *Inorg. Chem.* **2008**, *47*, 3958.

(47) van der Boom, M. E.; Milstein, D. *Chem. Rev.* **2003**, *103*, 1759.

(48) Bernskoetter, W. H.; Brookhart, M. *Organometallics* **2008**, *27*, 2036.

(49) Dani, P.; Karlen, T.; Gossage, R. A.; Gladiali, S.; van Koten, G. *Angew. Chem., Int. Ed.* **2000**, *39*, 743.

(50) Göttker-Schnetmann, I.; Brookhart, M. *J. Am. Chem. Soc.* **2004**, *126*, 9330.

(51) Göttker-Schnetmann, I.; White, P.; Brookhart, M. *J. Am. Chem. Soc.* **2004**, *126*, 1804.

(52) Göttker-Schnetmann, I.; White, P. S.; Brookhart, M. *Organometallics* **2004**, *23*, 1766.

(53) Gupta, M.; Hagen, C.; Flesher, R. J.; Kaska, W. C.; Jensen, C. M. *J. Chem. Soc., Chem. Commun.* **1996**, 2083.

(54) Jensen, C. M. *J. Chem. Soc., Chem. Commun.* **1999**, 2443.

(55) Krogh-Jespersen, K.; Czerw, M.; Summa, N.; Renkema, K. B.; Achord, P. D.; Goldman, A. S. *J. Am. Chem. Soc.* **2002**, *124*, 11404.

(56) Zhu, K.; Achord, P. D.; Zhang, X.; Krogh-Jespersen, K.; Goldman, A. S. *J. Am. Chem. Soc.* **2004**, *126*, 13044.

(57) Gandelman, M.; Milstein, D. *J. Chem. Soc., Chem. Commun.* **2000**, 1603.

(58) Liou, S.-Y.; van der Boom, M. E.; Milstein, D. *J. Chem. Soc., Chem. Commun.* **1998**, 687.

(59) Steenwinkel, P.; Gossage, R. A.; van Koten, G. *Chem.—Eur. J.* **1998**, *4*, 759.

(60) van der Boom, M. E.; Liou, S.-Y.; Ben-David, Y.; Shimon, L. J. W.; Milstein, D. *J. Am. Chem. Soc.* **1998**, *120*, 6531.

(61) Bedford, R. B.; Draper, S. M.; Scully, P. N.; Welch, S. L. *New J. Chem.* **2000**, *24*, 745.

(62) Beletskaya, I. P.; Chuchurjukin, A. V.; Dijkstra, H. P.; van Klink, G. P. M.; van Koten, G. *Tetrahedron Lett.* **2000**, *41*, 1075.

(63) Gorla, F.; Togni, A.; Venanzi, L. M.; Albinati, A.; Lianza, F. *Organometallics* **1994**, *13*, 1607.

(64) Longmire, J. M.; Zhang, X. *Tetrahedron Lett.* **1997**, *38*, 1725.

(65) Miyazaki, F.; Yamaguchi, K.; Shibasaki, M. *Tetrahedron Lett.* **1999**, *40*, 7379.

(66) Morales-Morales, D.; Grause, C.; Kasaoka, K.; Redón, R.; Cramer, R. E.; Jensen, C. *Inorg. Chim. Acta* **2000**, *300–302*, 958.

(67) Kaska, W. C.; Nemeh, S.; Shirazi, A.; Potuznik, S. *Organometallics* **1988**, *7*, 13.

(68) Vigalok, A.; Ben-David, Y.; Milstein, D. *Organometallics* **1996**, *15*, 1839.

(69) Nemeh, S.; Jensen, C.; Binamirasoriaga, E.; Kaska, W. C. *Organometallics* **1983**, *2*, 1442.

(70) Riddick, J. A.; Bunger, W. B.; Sakano, T. K. *Organic Solvents, Physical Properties and Methods of Purification*, 4th ed.; Wiley: New York, 1986.

(71) *Ethene*; Hayduk, W., Ed.; Solubility Data Series; Oxford University Press: Oxford, 1994; Vol. 57.

(72) Wilhelm, E.; Battino, R. *Chem. Rev.* **1973**, *73*, 1.

(73) *Nitrogen and Air*; Battino, R., Ed.; Solubility Data Series; Pergamon: Oxford, 1982; Vol. 10.

(74) *Hydrogen and Deuterium*; Young, C. L., Ed.; Solubility Data Series; Pergamon: Oxford, 1981; Vol. 5/6.

(75) Hayashi, Y.; Szalda, D. J.; Grills, D. C.; Hanson, J. C.; Huang, K.-W.; Muckerman, J. T.; Fujita, E. *Polyhedron*, in press, http://dx.doi.org/10.1016/j.poly.2012.10.006.

(76) Frisch, M. J.; et al. *Gaussian 03, Revision E.01*; Wallingford, CT, 2004.

(77) Hay, P. J.; Wadt, W. R. *J. Chem. Phys.* **1985**, *82*, 299.

(78) Hay, P. J.; Wadt, W. R. *J. Chem. Phys.* **1985**, *82*, 270.

(79) Wadt, W. R.; Hay, P. J. *J. Chem. Phys.* **1985**, *82*, 284.

(80) Dunning, T. H., Jr.; Hay, P. J. In *Modern Theoretical Chemistry*; Schaefer, H. F., III, Ed.; Plenum: New York, 1976; Vol. 3, pp 1.

(81) Martin, J. M. L.; Sundermann, A. *J. Chem. Phys.* **2001**, *114*, 3408.

(82) Andrae, D.; Häussermann, U.; Dolg, M.; Stoll, H.; Preuss, H. *Theor. Chim. Acta* **1990**, *77*, 123.

(83) Francl, M. M.; Pietro, W. J.; Hehre, W. J.; Binkley, J. S.; Gordon, M. S.; DeFrees, D. J.; Pople, J. A. *J. Chem. Phys.* **1982**, *77*, 3654.

(84) Harihara, P. C.; Pople, J. A. *Theor. Chim. Acta* **1973**, *28*, 213.

(85) Ehlers, A. W.; Böhme, M.; Dapprich, S.; Gobbi, A.; Höllwarth, A.; Jonas, V.; Köhler, K. F.; Stegmann, R.; Veldkamp, A.; Frenking, G. *Chem. Phys. Lett.* **1993**, *208*, 111.

(86) Roy, L. E.; Hay, P. J.; Martin, R. L. *J. Chem. Theory Comput.* **2008**, *4*, 1029.

(87) McLean, A. D.; Chandler, G. S. *J. Chem. Phys.* **1980**, *72*, 5639.

(88) Krishnan, R.; Binkley, J. S.; Seeger, R.; Pople, J. A. *J. Chem. Phys.* **1980**, *72*, 650.

(89) Frech, C. M.; Shimon, L. J. W.; Milstein, D. *Helv. Chim. Acta* **2006**, *89*, 1730.

(90) Bullock, R. M.; Bender, B. R. Isotope Methods in Homogeneous Catalysis. In *The Encyclopedia of Catalysis*; Horváth, I., Ed.; John Wiley & Sons: New York, 2002.

(91) Kubas, G. J. *Metal Dihydrogen and σ-Bond Complexes: Structure, Theory, and Reactivity*; Kluwer Academic/Plenum Publishers: New York, 2001; pp 222.

(92) Diffusion-controlled rate constants, k_d's, were estimated from the following equation, $k_d = 4\pi r^* D N_A$ (where r^* is the sum of the radii of the reactants, D is the sum of the diffusion constants, D of each reactant, and N_A is the Avogadro constant). Values of D were obtained

4171

dx.doi.org/10.1021/ic300672g | *Inorg. Chem.* 2013, 52, 4160−4172

from the Stokes−Einstein Equation, $D = k_B T/6\pi\eta r$ (where η is the viscosity of the solvent and r is the radius of the reactant).

(93) Although setting k_2 equal to the diffusion-controlled rate constant is an assumption, we believe that it is a reasonable one based on the initial slope fits, and also the fact that it involves the reaction of small incoming molecules with a nonsolvated, coordinatively unsaturated intermediate.

(94) van Eldik, R. High Pressure Kinetics: Fundamental and Experimental Aspects. In *Inorganic High Pressure Chemistry: Kinetics and Mechanisms*; van Eldik, R., Ed.; Elsevier: Amsterdam, 1986; Vol. 7, pp 8.

(95) Huang, K.-W.; Grills, D. C.; Han, J. H.; Szalda, D. J.; Fujita, E. *Inorg. Chim. Acta* **2008**, *361*, 3327.

(96) Perutz, R. N.; Turner, J. J. *J. Am. Chem. Soc.* **1975**, *97*, 4791.

(97) Kelly, J. M.; Long, C.; Bonneau, R. *J. Phys. Chem.* **1983**, *87*, 3344.

(98) Johnson, F. P. A.; George, M. W.; Bagratashvili, V. N.; Vereshchagina, L. N.; Poliakoff, M. *Mendeleev Commun.* **1991**, 26.

(99) Hodges, P. M.; Jackson, S. A.; Jacke, J.; Poliakoff, M.; Turner, J. J.; Grevels, F. W. *J. Am. Chem. Soc.* **1990**, *112*, 1234.

(100) van Eldik, R.; Meyerstein, D. *Acc. Chem. Res.* **2000**, *33*, 207.

(101) The same scheme will also be used to explain the reactivity of **1**. See details below.

(102) http://www.almaden.ibm.com/st/computational_science/ck/?cks

(103) Very low concentrations of N_2 were achieved through the use of specially prepared gas mixtures of Ar/N_2.